Role of point defects in the electrical and optical properties of In_2O_3

Intuon Chatratin,[1,2] Fernando P. Sabino,[1] Pakpoom Reunchan,[2,3,*] Sukit Limpijumnong,[4] Joel B. Varley,[5] Chris G. Van de Walle,[6] and Anderson Janotti[1,†]

[1]*Department of Materials Science and Engineering, University of Delaware, Newark, Delaware 19716, USA*
[2]*Department of Physics, Faculty of Science, Kasetsart University, Bangkok 10900, Thailand*
[3]*Thailand Center of Excellence in Physics (ThEP Center), Commission on Higher Education, Bangkok 10400, Thailand*
[4]*The Institute for the Promotion of Teaching Science and Technology, Bangkok 10110, Thailand*
[5]*Lawrence Livermore National Laboratory, Livermore, California 94550, USA*
[6]*Materials Department, University of California, Santa Barbara, California 93106-5050, USA*

(Received 24 May 2019; published 29 July 2019)

Using hybrid density-functional calculations we investigate the effects of native point defects on the electrical and optical properties of In_2O_3. We analyze formation energies, transition levels, and local lattice relaxations for all native point defects. We find that donor defects are in general more energetically favorable than acceptor defects, except near O-rich conditions, where oxygen interstitials and indium vacancies have low formation energy in *n*-type In_2O_3. The oxygen vacancy is the lowest-energy donor defect with transition level $(2+/+)$ slightly below and $(+/0)$ slightly above the conduction-band minimum (CBM), with a predicted luminescence peak at 2.3 eV associated with the transition $V_O^0 \rightarrow V_O^+$. Despite being a shallow donor, the oxygen vacancy becomes electrically inactive for Fermi levels at or higher than ∼0.1 eV above the CBM. This indicates that conductivity due to oxygen vacancies will saturate at rather low carrier concentrations when compared to typical carrier concentrations required for transparent conducting oxides in many device applications.

DOI: 10.1103/PhysRevMaterials.3.074604

I. INTRODUCTION

Materials that combine high optical transparency with high electrical conductivity are of great technological interest. They can be used as transparent electrodes in light-emitting diodes, solar cells, and flat-panel displays and as transparent heat-mirror coatings due to their high infrared (IR) reflectivity [1–4]. In_2O_3 belongs to this class of materials. When heavily doped with Sn, so-called ITO (Sn-doped In_2O_3) can support very high carrier densities (up to 10^{21} cm^{-3}) and still remain transparent with optical transmittance of over 80% in the region of visible light [5]. For applications as transparent electrodes, amorphous or polycrystalline In_2O_3 films, grown by large-area deposition techniques such as spray pyrolysis and sputtering, are often employed due to the relatively low cost of fabrication [2]. In_2O_3 can also be obtained as bulk single crystals [6,7], allowing for homoepitaxy of single crystalline films. The prospect of growing thin films with high crystal quality using techniques that also allow for controlling impurity incorporation makes In_2O_3 very attractive as a semiconductor in its own right. In addition to its importance for transparent electrodes, In_2O_3 has enormous potential for semiconductor device applications as long as one can master the control of *n*-type conductivity and, possibly, make it *p* type. Understanding the factors that control the often observed unintentional *n*-type conductivity [6,8,9] can also lead to improvements in the performance of In_2O_3-based transparent electrodes.

High levels of *n*-type conductivity, with carrier densities of 10^{17}–10^{20} cm^{-3}, in nominally undoped In_2O_3 bulk single crystals and thin films have been extensively reported in the literature [8–12]. However, the cause of the unintentional *n*-type conductivity in In_2O_3 is still a subject of debate [13–17]. Similarly to other oxides, such as ZnO and SnO_2, the unintentional *n*-type conductivity in In_2O_3 has been traditionally attributed to the presence of native point defects, such as O vacancies or In interstitials. The arguments usually rely on the dependence of the conductivity on the oxygen partial pressure in the growth or annealing environments [18–24]. However, in the case of ZnO and SnO_2, it has been shown that O vacancies cannot cause conductivity because they are deep donors [14, 25–27]. In addition, cation interstitials, although predicted to act as shallow donors, have high formation energies and are typically fast diffusers, making them unstable [25]. These results raise the question of whether native point defects actually play any role in the observed unintentional *n*-type conductivity in In_2O_3.

From a theory perspective, the apparent confusion regarding the role of point defects in the electrical conductivity in In_2O_3 [13–15,22,28,29] is largely due to the severe underestimation of the band gap in the widely employed functionals within the density-functional theory (DFT) as well as the different approaches used to overcome this problem. In In_2O_3, the fundamental band gap is ∼0.8 eV lower than the optical band gap due to weak or dipole-forbidden transitions from higher states in the valence band to the lowest-energy conduction band [30,31]. While the experimental value for the

*pakpoom.r@ku.ac.th
†janotti@udel.edu

fundamental band gap is in the range 2.7–2.9 eV [30,32,33], functionals such as the local density approximation (LDA) or the generalized gradient approximation (GGA) produce values of only about 1.0 eV [28].

Tanaka *et al.* [29] performed DFT-GGA calculations for neutral O vacancies in In_2O_3. They reported a formation energy of −1.07 eV for the neutral O vacancy in the O-poor limit. After an *ad hoc* correction in which the doubly occupied state induced by the vacancy is assumed to shift upward with the conduction band as the band gap is corrected, the formation energy is increased to 3.80 eV. Recently, Tomita *et al.* [22] performed calculations for native point defects in In_2O_3 clusters by using the discrete variational Xα molecular orbital method [34]. They concluded that O vacancies cannot cause conductivity because the related doubly occupied single-particle state, located at 2.46 eV above the valence band, is well below the conduction-band minimum (CBM). Note that Tomita *et al.* [22] assumed a band gap of 3.75 eV for bulk In_2O_3. In addition, O vacancies in In_2O_3 are expected to display very different local lattice relaxations for different charge states, as in the case of ZnO [25] and SnO_2 [26]; in this case the single-particle states do not coincide with the thermodynamic transition levels, and it is the latter that ultimately determine ionization energies.

Lany and Zunger [13] also performed DFT calculations for point defects in In_2O_3 and concluded that O vacancies are deep donors with the (2+/0) transition level at 2.3 eV above the valence band, assuming a band-gap value of 3.7 eV for In_2O_3 [35]. They applied corrections to the DFT transition levels by using GGA + U, assuming that the latter only corrects the position of the valence-band maximum (VBM). This assumption has been shown to be unfounded in the case of ZnO [25] and is not expected to hold in the case of In_2O_3 either: The GGA + U affects the position of both valence band and conduction band [36]. Ágoston *et al.* [15] performed GGA + U calculations for native defects in In_2O_3 and concluded that oxygen vacancies are shallow donors, based on a calculated band gap of 1.79 eV. An extrapolation based on LDA and LDA + U indicated that the oxygen vacancy has the donor level (2+/0) at 0.2 eV below the conduction band [28,37]. More recent GGA + U calculations predicted much deeper donor transition levels for oxygen vacancies [38]. Ágoston *et al.* [14] reported results of hybrid functional calculations for oxygen vacancies in In_2O_3 and concluded that oxygen vacancies are shallow donors with the (2+/0) level above the CBM. Shallow donor behavior of oxygen vacancies in orthorhombic In_2O_3 has also also reported [39]. On the other hand, using a similar functional, oxygen vacancies were reported to be deep donors by other groups [40,41].

Most recently, based on a hybrid quantum mechanical–molecular mechanical embedded cluster approach, Buckeridge *et al.* [16] argued that the oxygen vacancy in In_2O_3 is a shallow donor, with (2+/+) and (+/0) above the CBM, and can account for the observed carrier concentrations of 10^{18}–10^{20} cm^{-3} [18–20,23,24]. Their conclusions, for both O-rich and O-poor limits, were based on a charge neutrality analysis that only takes into account oxygen vacancies, completely neglecting the effects of compensating acceptor defects such as the In vacancy and O interstitial. These defects are expected to dominate under O-rich conditions and Fermi level position near the conduction band, as discussed below.

TABLE I. Calculated lattice parameter, band gap, and enthalpy of formation for In_2O_3 in the bixbyite phase. Both DFT-LDA and HSE results are listed along with the experimental values.

Property	LDA	HSE	Exp.
a (Å)	10.07	10.19	10.12 [50]
E_g (eV)	1.17	2.79	2.7–2.9 [30,33,52,53]
ΔH_f (eV)	−9.86	−8.19	−9.59 [54]

Given that previous work has produced contradicting results and conclusions, we consider it important and timely to revisit the issue of the role of native point defects in n-type conductivity of In_2O_3 and also discuss how they may affect attempts to achieve p-type doping. We use the screened hybrid functional of Heyd, Scuseria, and Ernzenhof (HSE) [42,43] to calculate formation energies, transition levels, and local lattice relaxations for all native point defects in In_2O_3. Although HSE has already been used to study the oxygen vacancy, In interstitial, and O interstitial [14,44], a comprehensive picture including all native point defects using the same functional is still missing in the literature. We also studied the optical properties of native defects, focusing on the luminescence associated with indium and oxygen vacancies to aid in the experimental efforts to identify these defects. Note that HSE describes band gaps much more accurately than the traditional DFT-LDA or GGA functionals, resulting in defect formation energies and transition levels that can be directly compared to experiments [45].

II. COMPUTATIONAL APPROACH

Our calculations are based on generalized Kohn-Sham scheme with the HSE-screened hybrid functional and the projector-augmented-wave method as implemented in the VASP code [42,46–49]. We use a Hartree-Fock mixing parameter of 0.28 and a standard screening length of 10 Å, giving band-gap and equilibrium lattice parameters in good agreement with experimental data, as listed in Table I. We use periodic boundary conditions with a supercell of 80 atoms for the In_2O_3 bixbyite structure. For the integrations over the Brillouin zone, we use the (1/4,1/4,1/4) special k point; tests using a $2 \times 2 \times 2$ k-mesh indicate that total energy differences are converged within 0.1 eV. For the plane-wave basis set, we use a cutoff of 400 eV. All the atoms are allowed to relax until the forces are less than 0.015 eV/Å, and all the defect calculations include spin polarization. The effects of finite supercell size on the formation energies of charged defects were corrected as described in Ref. [51].

Defect formation energies and transition levels

The formation energy of a defect X in charge state q in In_2O_3 is given by [45]:

$$E^f(X^q) = E_{\rm tot}(X^q) - E_{\rm tot}(In_2O_3) + n_{\rm In}E_{\rm tot}({\rm In}) + n_{\rm O}[1/2E_{\rm tot}(O_2)] + n_{\rm In}\mu_{\rm In} + n_{\rm O}\mu_{\rm O} + q(\varepsilon_F + \varepsilon_{\rm VBM}) + \Delta^q, \quad (1)$$

where $E_{\rm tot}(X^q)$ is the total energy of the supercell containing the defect X in charge state q, and $E_{\rm tot}(In_2O_3)$ is the total energy of the perfect crystal in the same supercell. The integers $n_{\rm In}$ and $n_{\rm O}$ are the number of O and In atoms that are added to or removed from the perfect crystal to form the defect. The chemical potentials $\mu_{\rm In}$ and $\mu_{\rm O}$ represent the energy of the reservoir for In and O atoms and referenced to the total energy per atom of the respective standard phase. In the case of In, the standard phase is In bulk [$E_{\rm tot}$(In)], and in the case of O it is an O_2 molecule [$1/2E_{\rm tot}(O_2)$]. Since defects can occur in charge states other than neutral, the formation energy also depends on the position of the Fermi level ε_F, which represents the energy of the electron reservoir in the material. We follow the convention of referencing ε_F to the VBM of the host material ($\varepsilon_{\rm VBM}$). The last term contains the alignment of the VBM in the perfect crystal with the defects supercell and the charge-state dependent correction for the finite size of the supercell [51].

From Eq. (1), we can see that the formation energy of native point defects in In_2O_3 varies with the chemical potentials $\mu_{\rm In}$ and $\mu_{\rm O}$, which can be chosen to correspond to the O-poor (In-rich) or O-rich (In-poor) limits or anything in between. The chemical potentials $\mu_{\rm In}$ and $\mu_{\rm O}$ are not independent, since they must satisfy stability condition of In_2O_3:

$$2\mu_{\rm In} + 3\mu_{\rm O} = \Delta H_f(In_2O_3), \tag{2}$$

where $\Delta H_f(In_2O_3)$ is formation enthalpy of In_2O_3. In the O-poor limit we have $\mu_{\rm In} = 0$ and $\mu_{\rm O} = 1/3\Delta H_f(In_2O_3)$; in the O-rich limit we have $\mu_{\rm O} = 0$ and $\mu_{\rm In} = 1/2\Delta H_f(In_2O_3)$. The Fermi level position at which the formation energy of a defect in the charge q [$E^f(X^q)$] equals the formation energy of the same defect in the charge state q' [$E_f(X^{q'})$] defines the thermodynamic transition level (q/q'),

$$(q/q') = \frac{E^f(X^q;\varepsilon_F = 0) - E^f(X^{q'};\varepsilon_F = 0)}{q' - q}, \tag{3}$$

where $E^f(X^q;\varepsilon_F = 0)$ is the formation energy of X^q taken at $\varepsilon_F = 0$. These transition levels (q/q') are not to be confused with optical transition levels in which the electronic transition $X^q \rightarrow X^{q'}$ is much faster than typical lattice vibrations so that the lattice does not have time to relax to the equilibrium structure of $X^{q'}$. Optical transition levels are determined from configuration coordinate diagrams as described in Ref. [45].

III. RESULTS AND DISCUSSION

We investigated all possible native point defects in In_2O_3: oxygen and indium vacancies ($V_{\rm O}$ and $V_{\rm In}$), interstitials (O_i and In_i), and antisites ($O_{\rm In}$ and $In_{\rm O}$). In this section we discuss the results for formation energies and the donor-acceptor behavior as function of the Fermi level position, including for n-type material, where ε_F is near the CBM, and for p-type material, where ε_F is near the VBM. We also present detailed information on the local lattice relaxations and distortions related to the defects. In addition to electrical properties, the optical properties of indium and oxygen vacancies are also considered. Note that in the In_2O_3 bixbyite structure there are two nonequivalent In sites, the 8b site (1/4, 1/4, 1/4) (In1) and the 24d site (u, 0, 1/4) (In2), and only one type of O site, the 48e site (x, y, z), following the Wyckoff notation (see Fig. 1).

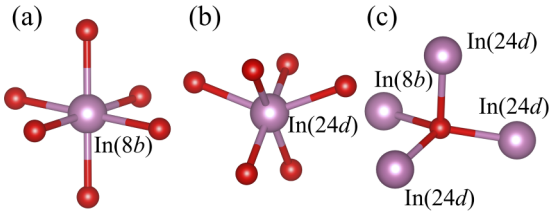

FIG. 1. Local lattice structure around In and O atoms in bixbyite In_2O_3. There are two inequivalent sites for In atoms, (a) the 8b site and (b) the 24d site, labeled In(8b) and In(24d), respectively. (c) Oxygen atoms are surrounded by one In(8b) and three In(24d) atoms.

Figure 2 shows the formation energies as a function of the Fermi level ε_F for all native point defects in In_2O_3. The results for the O-poor limit are in Fig. 2(a) and for the O-rich limit in Fig. 2(b). The defects with lowest formation energies, and thus the most relevant, in O-poor conditions are $V_{\rm O}$, In_i, and $In_{\rm O}$, for all Fermi-level positions in the gap. In O-rich conditions, the lowest energy defects are O_i, $V_{\rm In}$, and $O_{\rm In}$ when the Fermi level is near the CBM, and $V_{\rm O}$, In_i, and O_i for Fermi-level positions in the lower part of the band gap.

Note that in O-rich conditions, donor defects have higher formation energies than acceptor defects for Fermi level near the CBM; therefore, we expect that native defects will not lead to conductivity. In O-poor conditions, on the other hand, donor defects are more favorable for all Fermi level positions across the band gap, remaining uncompensated. In this case, it is possible that native defects will lead to n-type conductivity.

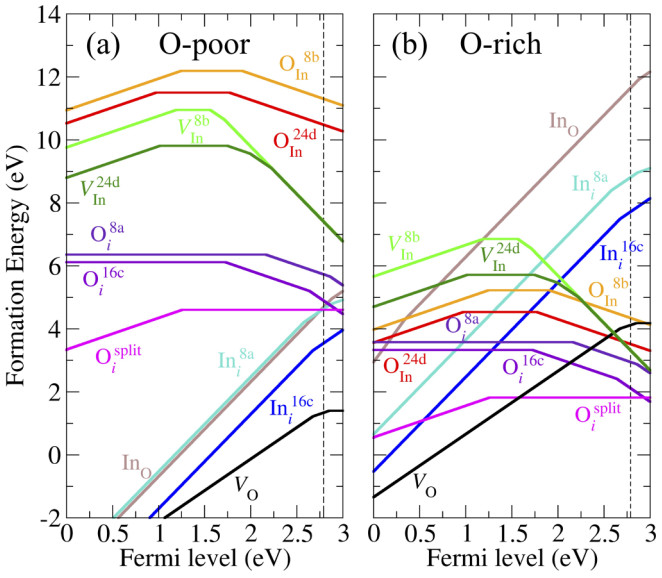

FIG. 2. Formation energies as a function of Fermi level position for native point defects in In_2O_3. Results are shown for (a) the O-poor limit and (b) the O-rich limit. The zero of Fermi level corresponds to the VBM and the dashed line indicates the CBM. Only segments corresponding to the lowest energy charge states are shown. The slope of each segment indicates the charge state. Kinks in the lines for the same defect indicate the thermodynamic transition levels.

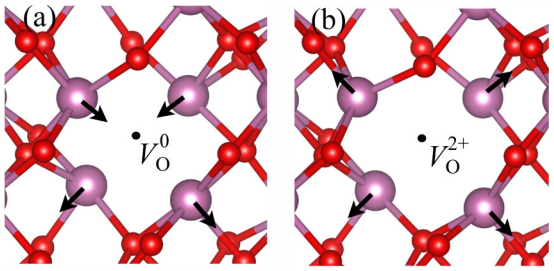

FIG. 3. Local lattice relaxations around the oxygen vacancy in the (a) neutral charge state (V_O^0) and (b) 2+ charge state (V_O^{2+}). In the neutral charge state (V_O^0), two In nearest neighbors are displaced inward, while the other two are displaced outward away from the vacancy site. In the 2+ charge state (V_O^{2+}), all four In atoms are displaced outward.

We also note that in both O-rich and O-poor conditions, donor defects are strongly favorable as the Fermi level approaches the valence band, indicating they may play an important role as compensation centers in attempts to dope In_2O_3 with acceptor impurities. In the following subsections we discuss the properties of each defect.

A. Oxygen vacancies (V_O)

The O atoms in In_2O_3 are surrounded by four In nearest neighbors, with four slightly different In-O bond lengths (2.15, 2.19, 2.21, and 2.22 Å). The removal of an O atom to form a vacancy results in four In dangling bonds and a total of two electrons. These four In dangling bonds combine into a lower energy a_1 state in the band gap and three almost-degenerate higher energy states located in the conduction band. In the neutral charge state (V_O^0), the a_1 state is doubly occupied and located at 0.44 eV below the CBM. Two of the four In nearest neighbors relax inward by 1.4% and 4.7% but the two other are displaced outward by 2.3% and 3.2% of their equilibrium In-O bond length, as shown in Fig. 3(a). In the 1+ charge state (V_O^+), the singly occupied (spin-up) a_1 state is at 0.37 eV below the CBM and the In nearest neighbors relax outward by 3.3%, 5.0%, 5.4%, and 8.1%. Finally, in the 2+ charge state (V_O^{2+}) the a_1 state is empty and resonant in the conduction band and the In nearest neighbors significantly relax outward by 9.3%, 9.6%, 7.7%, and 13%. This behavior is qualitatively similar to the case of V_O in ZnO, except that for V_O^0 all four Zn nearest neighbors relax inward [25].

The formation energies for V_O in In_2O_3 as a function of ε_F are shown in Fig. 2. We find the (2+/+) transition level at 0.11 eV below the CBM and the (+/0) level at 0.06 eV above the CBM. We verified that the a_1 state is correctly occupied in the calculations of V_O^0 and V_O^+. Hence, our calculations indicate that V_O is a shallow donor in In_2O_3 and that, assuming that the oxygen vacancy is the dominant defect-impurity, most of the vacancies will be singly ionized and only a small fraction will be doubly ionized at room temperature considering the (2+/+) level of 0.11 eV. Note that oxygen vacancies will not lead to high electron concentrations, as required in typical transparent conducting oxides (TCO) applications [2], because at $\varepsilon_F > 0.06$ eV above the CBM, these vacancies will be more stable in the neutral charge state, i.e., they will be electrically inactive. Therefore, we expect the conductivity due to the oxygen vacancies to saturate, limiting the carrier concentration. This result also explains why the reported Hall carrier concentrations is limited to less than 5×10^{17} cm^{-3} in undoped In_2O_3 films grown by molecular beam epitaxy (MBE) under slightly In-rich conditions [8].

The narrow range in Fermi level for the stability of V_O^+, reflecting a relatively weak Coulomb repulsion for adding a second electron to form V_O^0, is consistent with the very different lattice relaxations for the neutral, 1+, and 2+ charge states. The low or even negative formation energies of V_O^{2+} for ε_F approaching the VBM (in both O-rich and O-poor conditions) indicate that oxygen vacancies will strongly compensate acceptor dopants, limiting or precluding *p*-type conductivity in In_2O_3. This result explains the experiments of Bierwagen and Speck [55] where Mg acceptors in MBE grown In_2O_3 films were found to be fully compensated.

The difference between the present results and previous HSE calculations for the oxygen vacancy can be attributed to the lower Hartree-Fock mixing parameter [14,40,41], the method employed for the charge-state-dependent supercell-size correction, and the choice of *k*-point sampling [14,40]. The results from the smaller Hartree-Fock mixing parameters yield lower energy gaps and a lower (2+/0) transition level. The lower mixing parameter may also explain the absence of a 1+ charge state in the previous reports [14,40,41] since the 1+ charge state is stable only in a very narrow range of Fermi levels.

One way to detect oxygen vacancies in In_2O_3 would be through photoluminescense experiments. Assuming *n*-type samples where the conductivity is attributed to a high concentration of intentionally added shallow donor impurities, which would push the Fermi level to more than 0.06 eV above the CBM, oxygen vacancies will be stable in the neutral charge state. After UV light excitation that creates electron-hole pairs, an electron from the vacancy a_1 state recombines with a hole in the valence band, emitting a photon (i.e., $V_O^0 + h \rightarrow V_O^+ + \hbar\omega$). The optical transition of this process is obtained from the calculated configuration coordinate diagram shown in Fig. 4. Due to the difference in local lattice relaxations of V_O^0

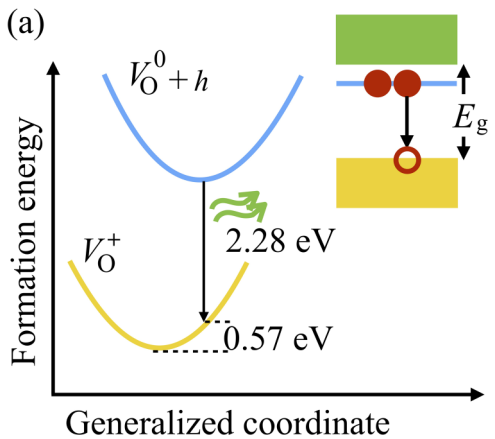

FIG. 4. Calculated configuration coordinate diagram for the optical transition $V_O^0 + h \rightarrow V_O^+$, where h represents a free hole in the valence band created under light excitation.

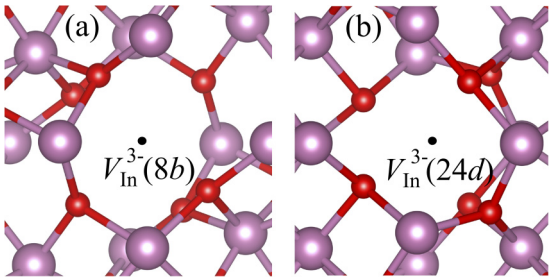

FIG. 5. Local atomic geometry of the indium vacancy in the 3- charge state in the (a) the 8*b* site [$V_{In}^{3-}(8b)$] and (b) the 24*d* site [$V_{In}^{3-}(24d)$] in In_2O_3.

and V_O^+, we predict a broad emission peak centered at 2.3 eV. Recent photoluminescense measurements by Beji *et al.* [56] on In_2O_3 thin films reveal a broad peak centered at ∼2.3 eV (530 nm), but they do not address the microscopic origin. Based on the agreement with our predicted 2.3-eV peak, we suggest it is due to oxygen vacancies.

We note that holes can be self-trapped in In_2O_3, with a self-trapping energy of 0.25 eV and a barrier to self-trapping of 0.14 eV [57]. This could make it difficult to observe the predicted 2.3-eV peak. However, given the barrier to self-trapping, free holes (i.e., holes that do not get self-trapped) are likely to be available for the recombination process with a 2.3-eV emission peak.

B. Indium vacancies (V_{In})

Each In atom in In_2O_3 is surrounded by six O atoms. There are two nonequivalent In sites in the In_2O_3 bixbyite structure, labeled 8*b* and 24*d*, as shown in Fig. 1. The removal of an In atom to form a vacancy, V_{In}, results in six O dangling bonds with a total of three electrons. These dangling bond sates combine into partially occupied gap states with three holes (missing electrons). Possible charge states of V_{In} are 1+, neutral, 1−, 2−, and 3−. For both nonequivalent In sites, the O atoms surrounding the V_{In} are too far apart to form O-O chemical bonds as shown in Fig. 5. Instead, we find that the six nearest-neighbor O atoms significantly relax outward by 6–12% of the average In-O equilibrium bond length, with the largest relaxations being observed for V_{In}^{3-}.

We find that the formation energy of $V_{In}^0(8b)$ is about 1 eV higher than that of $V_{In}^0(24d)$, as shown in Fig. 2, while the formation energy of $V_{In}^{3-}(8b)$ is very close to that of $V_{In}^{3-}(24d)$. Thus, the positions of the (0/−), (−/2−), and (2−/3−) transition levels of $V_{In}(24d)$ are different from those of $V_{In}(8b)$. For $V_{In}(24d)$, (0/−), (−/2−), and (2−/3−) levels are at 1.75, 1.99, and 2.22 eV above the VBM, while for $V_{In}(8b)$ they are at 1.55, 1.56, and 1.71 eV above the VBM, respectively. In the case of V_{In}^- and V_{In}^0 we find that high-spin states ($S = 1$ and $S = 3/2$, respectively) are more favorable than low-spin states.

The present results differ somewhat from previous HSE calculations [58]. We attribute this difference to the lower mixing parameter for the Hartree-Fock exchange used in the present work. Here the band gap is 2.79 eV (mixing parameter 28%) while in the previous work the calculated band gap was 3.04 eV (mixing of 32%) [58]. The higher mixing parameter leads to a lower VBM. We also predict the formation energy for $V_{In}^0(8b)$ to be higher than previous results, which we also attribute to the difference in mixing parameter. Higher mixing parameter leads to less stable In metal with respect to the oxide, thus lowering the formation energy of the In vacancy. The lower formation energy of $V_{In}^0(24)$ with respect to $V_{In}^0(8b)$ can be attributed to lower symmetry of the vacancy in the In(24d) site in our calculations.

The formation energy of V_{In}^{3-} is low only under O-rich conditions and for ε_F near the conduction band. In this case, V_{In}^{3-} is a compensating center in *n*-type In_2O_3, especially in samples where the Fermi level is located well above the CBM, i.e., in TCO films with high carrier concentrations. In moderately *n*-type doped In_2O_3, where ε_F is close to the CBM, the lowest energy acceptor defects are oxygen interstitials, as discussed below, and V_{In}^{3-} plays only a secondary role as a compensating acceptor. This observation can explain recent positron annihilation spectroscopy experiments [59] which have indicated that oxygen annealing leads to an increase in In vacancy concentration, yet the vacancy is not the main compensating acceptor. On the other hand, V_{In} have very high formation energies when ε_F approaches the VBM and, consequently, will be unlikely to be present even in samples annealed or grown under O-rich conditions. However, note that previous calculations have indicated that interactions with hydrogen impurities, which can be unintentionally incorporated, can significantly bring down the formation energy of In vacancies [58] due to the formation of O-H bonds, making the vacancies even more relevant as compensation centers of *n*-type conductivity.

We also calculated the optical transitions associated with the In vacancy. Since most In_2O_3 samples are *n* type, we considered a situation where an electron is lifted from the gap state associated with V_{In}^{3-} on light excitation; i.e., we calculated the emission energy due to the recombination of a conduction-band electron and a hole in the V_{In}^{3-} gap state ($V_{In}^{2-} + e^- \rightarrow V_{In}^{3-} + \hbar\omega$). For $V_{In}(8b)$, the calculated emission peak energy is 0.67 eV, as illustrated in the configuration coordinate diagram in Fig. 6(a). For $V_{In}(24d)$, we find that the electron-hole recombination is nonradiative with a small thermal barrier of 10 meV [Fig. 6(b)].

C. Oxygen interstitials (O_i)

Extra O atoms can, in principle, also occupy the 16*c* or 8*a* interstitial sites in In_2O_3. We also find that an O atom placed at the 8*a* interstitial site can form a split-interstitial pair with one of the surrounding O atoms. In this configuration, the two O atoms share the same lattice site, with an O-O bond length of 1.46 Å, suggesting the formation of an O_2 molecule as shown in Fig. 7(a). The electronic structure of the O split interstitial resembles that of an O_2 molecule; the π^* antibonding state, from a molecular orbital description, is located in the band gap and completely occupied in the neutral charge state, resembling an O_2^{2-} molecule. This explains the longer O-O bond length found in the O split interstitial as compared to the value in the isolated O_2 molecule. Note that the structure and electronic properties of the oxygen split interstitial in In_2O_3 are similar to the model of diatomic molecules involving

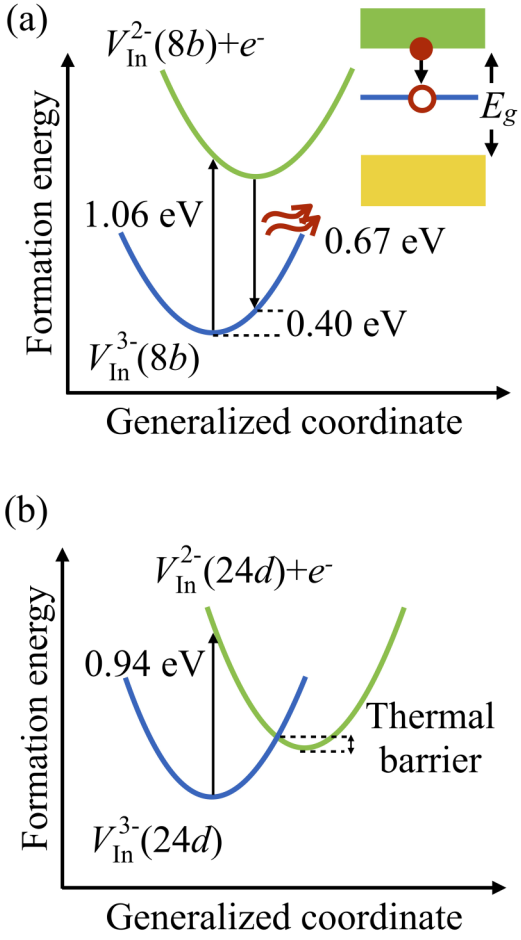

FIG. 6. Calculated configuration coordinate diagram for (a) the optical transition $V_{In}^{2-}(8b) + e^- \rightarrow V_{In}^{3-}(8b)$ assuming an electron was initially lifted from the $V_{In}^{3-}(8b)$-related state in the gap, then an electron from the conduction band e^- recombines with the hole in the $V_{In}^{2-}(8b)$, resulting in $V_{In}^{3-}(8b)$. In the case of (b) $V_{In}^{3-}(24d)$, a nonradiative recombination is predicted with a thermal barrier of 10 meV.

first-row elements in ZnO, as discussed in Ref. [60]. We find a (+/0) transition level at 1.26 eV above the valence band, and hence the O split interstitial is electrically inactive in *n*-type In_2O_3.

Besides the split interstitial configuration, we find that O can also be stable at the 16*c* or 8*a* interstitial sites in In_2O_3, as shown in Fig. 7. In the neutral charge state, O_i at the 16*c*

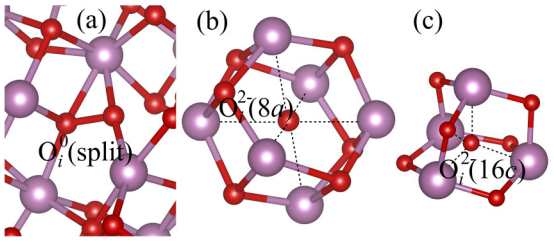

FIG. 7. Local atomic geometry of (a) the neutral split oxygen interstitial [$O_i^0(split)$] and the oxygen interstitial in a 2- charge state at (b) the 8*a* site [O_i^{2-}(8a)] and (c) the 16*c* site [O_i^{2-}(16c)].

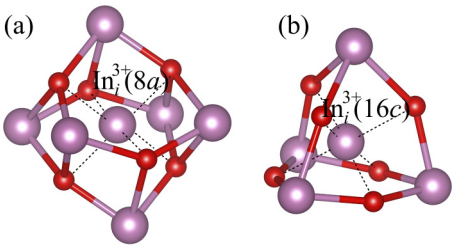

FIG. 8. Local atomic positions around the indium interstitial in the 3+ charge state (In_i^{3+}) at the (a) 8*a* site and (b) 16*c* site in the bixbiyte structure of In_2O_3.

site is only 0.2 eV lower in energy than at the 8*a* site. The O_i at both of these intersititial sites act as very deep acceptors; for 16*c* the (0/−) and (−/2−) transition levels are at 1.72 and 2.64 eV above the VBM, while for 8*a* they are at 2.16 and 2.86 eV above the VBM. Note that O_i at the 16*c* site is the lowest energy acceptor defect under O-rich conditions, acting as a compensating center in *n*-type In_2O_3.

D. Indium interstitials (In_i)

In bixbyite In_2O_3 there are two nonequivalent interstitial sites, labeled 8*a* and 16*c* according to the Wyckoff notation. The interstitial sites 8*a* are surrounded by six In atoms and six O atoms in an octahedral environment as shown in Fig. 8(a). The interstitial sites 16*c* are surrounded by four In atoms and six O atoms as shown in Fig. 8(b).

For both 8*a* and 16*c* sites, we find that In_i leads to states located near the conduction band. As shown in Fig. 1, we find that In_i is mostly stable in the 3+ charge states for Fermi level positions across the gap, except very close to the conduction band, with the In_i^{3+}(16*c*) being 1.2 eV lower in energy than the In_i^{3+}(8*a*). For In_i(8*a*) we find the (3+/2+) transition level at 0.21 eV below the CBM, and the (2+/+) level at 0.07 eV above the CBM, whereas for the In_i(16*c*) we find the (3+/2+) level at 0.11 eV below the CBM. Regarding the local lattice relaxations, we find that In_i is only slightly displaced from the ideal interstitial sites with noticeable outward (inward) displacements of the surrounding In (O) atoms.

We find that In_i have formation energies that are significantly higher than that of oxygen vacancy for ε_F near the CBM, even in O-poor conditions. These high formation energies indicate that In interstitials are unlikely to be present in significant concentrations in *n*-type In_2O_3 under equilibrium conditions. On the other hand, their formation energy is very low for ε_F in the lower part of the band gap, indicating that In_i^{3+} may be an important compensating center in acceptor-doped In_2O_3, along with V_O^{2+}.

Similarly to zinc interstitials in ZnO [25], In_i is expected to be highly mobile in In_2O_3 [61]. In this case it would be unlikely that In_i would exist as isolated defects, even if introduced through nonequilibrium techniques such as ion implantation. Under those conditions, one could generate In_i, and they would diffuse and bind to other defects or impurities (at room temperature) and form complexes that are stable, unless the material is annealed at high-enough temperatures to break the complex. Therefore, we are led to conclude that

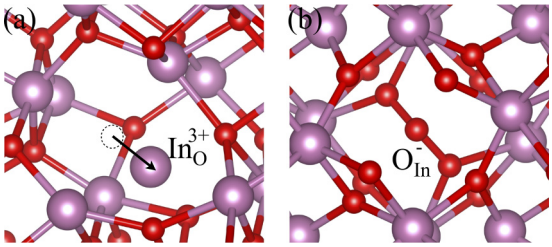

FIG. 9. Local atomic geometry of (a) the indium antisite in the 3+ charge state (In_O^3+) and (b) the oxygen antisite in the − charge state (O_{In}^-).

isolated In_i cannot be responsible for the unintentional *n*-type conductivity that is often observed in In_2O_3.

E. Indium antisites (In_O)

We find that In occupying O lattice sites is subjected to large off-site displacements. The In atom is displaced along the $[\bar{1}1\bar{1}]$ direction by 1.2 Å from the O substitutional site toward three next-nearest-neighbor O atoms, as shown in Fig. 9(a). In the relaxed configuration of In_O^{3+}, the In_O-O bond lengths are only ∼4% larger from the average In-O equilibrium bond length. This configuration can be understood as an In_i-V_O complex, as in the case of Zn antisite in ZnO [25]. The high-energy a_1 state related to In_i couples with the a_1 gap state related to V_O, stabilizing the complex.

Although In_O is a shallow donor, it has very high formation energy when ε_F is near the conduction band. Its formation energy is comparable to that of $In_i^{3+}(8a)$ in the O-poor limit but much higher in O-rich conditions. We thus conclude that In_O cannot explain the observed *n*-type conductivity in In_2O_3 due to the extremely high formation energy when ε_F is near the conduction band.

F. Oxygen antisites (O_{In})

Since In_2O_3 has two nonequivalent In sites, we investigated the possibility of O occupying the 8*b* or the 24*d* lattice sites. In both cases, we find that O_{In} are characterized by large off-site displacements toward two of the four nearest-neighbor O atoms, as shown in Fig. 9(b). We also find that O_{In} at the 24*d* site is lower in energy than at the 8*b* site.

In the relaxed configuration, O_{In} is bonded to two nearest-neighbor atoms with bond lengths in the range of 1.29–1.45 Å and O-O_{In}-O angles in the range of 110°–114°. O_{In} is amphoteric, i.e., it acts as acceptor for ε_F near the CBM and as a donor for ε_F near the VBM, with transition levels (+/0) = 0.97 eV and (0/−) = 1.77 eV above the VBM for the 24*d* site and (+/0) = 1.25 eV and (0/−) = 1.91 eV for the 8*b* site. The formation energies of O_{In} on both sites are very high in both In-rich and O-rich conditions. Hence, we expect the concentration of O_{In} to be negligible in In_2O_3 under equilibrium conditions. If introduced under nonequilibrium conditions, such as irradiation, then O_{In} will behave as a compensating center for both donor and acceptor impurities.

IV. SUMMARY

We performed a comprehensive investigation of the impact of native point defects on the electrical conductivity and optical properties of In_2O_3. We find that the unintentional *n*-type conductivity often observed in In_2O_3 can in principle be explained by the presence of oxygen vacancies when conditions are O-poor. In this case, we predict that most of oxygen vacancies will be singly ionized at room temperature with a (2+/+) transition level at 0.11 eV below the conduction band. Our results also show that conductivity due to oxygen vacancies tend to saturate as the (+/0) transition level is only 0.06 eV above the CBM, i.e., for high electron concentrations where the Fermi level is a few hundreds of meV or higher in the conduction band, oxygen vacancies will be electrically inactive. Oxygen vacancies give rise to a luminescence peak at 2.3 eV, corresponding to the transition from a vacancy-related state high in the gap to a hole in the VBM, resulting in a singly ionized vacancy.

In vacancies are deep acceptors with (2−/3−) transition levels in the upper part of the gap. They have relatively high formation energies for Fermi level within the gap, even in O-rich conditions. The vacancy in the 8*b* site will give rise to a luminescence peak at ∼0.7 eV after excitation of one electron from the vacancy-related gap state to the conduction band, while the vacancy in the 24*d* site is predicted to recombine nonradiatively. Interactions with hydrogen impurities would significantly lower their formation energy, as previously reported, making the complexes important compensating centers for *n*-type conductivity.

The oxygen interstitial at the 16*c* site is a deep acceptor with a (−/2−) transition level very close to the conduction band, while in the split interstitial configuration is electrically neutral for Fermi level in the upper part of the gap. These two forms compete in *n*-type In_2O_3, and the first is predicted to be the lower energy acceptor, which can be an especially relevant compensating center in O-rich conditions. Interstitials are shallow donors but have high formation energies in *n*-type In_2O_3 and are not expected to occur as isolated defects due to low migration barriers. If introduced under nonequilibrium processes, In_i would diffuse and form complex with other defects or impurities. Indium antisites are also shallow donors; however, their formation energy is also very high in *n*-type In_2O_3, even for extreme In-rich conditions. In_O can be understood as a complex between In_i and V_O. In vacancies and O interstitials are deep acceptors and act as compensating centers in *n*-type In_2O_3. Oxygen antisites are amphoteric and may be relevant if created under nonequilibrium conditions.

Finally. we predict an optical emission peak energy at 530 nm associated with the oxygen vacancy, which can explain a peak observed in the photoluminescence spectra of In_2O_3 thin films.

ACKNOWLEDGMENTS

This work was supported by the National Science Foundation Faculty Early Career Development Program No. DMR-1652994. P.R. acknowledges the Thailand Research Fund (Grant No. RSA6280068) and Kasetsart University Research and Development Institute (KURDI). C.G.V.d.W. acknowledges the GAME MURI of the Air Force Office of Scien-

tific Research (FA9550-18-1-0479). This work made use of the Extreme Science and Engineering Discovery Environment (XSEDE) facility, National Science Foundation Grant No. ACI-1053575, and the Information Technologies (IT) resources at the University of Delaware, specifically the high performance computing resources.

[1] K. L. Chopra, S. Major, and D. K. Pandya, Thin Solid Films **102**, 1 (1983).
[2] D. S. Ginley and C. Bright, Mater. Res. Bull **25**, 15 (2000).
[3] I. Hamberg and C. G. Granqvist, J. Appl. Phys. **60**, R123 (1986).
[4] M. Y. Tsai, O. Bierwagen, and J. S. Speck, Thin Solid Films **605**, 186 (2016).
[5] Y. Shigesato, in *Handbook of Transparent Conductors*, edited by D. S. Ginley, H. Hossono, and D. C. Paine (Springer, New York, 2010), Chap. 5, pp. 149–169.
[6] Z. Galazka, R. Uecker, K. Irmscher, D. Schulz, D. Klimm, M. Albrecht, M. Pietsch, S. Ganschow, A. Kwasniewski, and R. Fornari, J. Cryst. Growth **362**, 349 (2013).
[7] Z. Galazka, R. Uecker, and R. Fornari, J. Cryst. Growth **388**, 61 (2014).
[8] O. Bierwagen and J. S. Speck, Appl. Phys. Lett. **97**, 072103 (2010).
[9] O. Bierwagen, Semicond. Sci. Technol. **30**, 024001 (2015).
[10] R. L. Weiher, J. Appl. Phys. **33**, 2834 (1962).
[11] H. K. Müller, Phys. Status Solidi B **27**, 723 (1968).
[12] J. H. W. de Wit, J. Solid State Chem. **8**, 142 (1973).
[13] S. Lany and A. Zunger, Phys. Rev. Lett. **98**, 045501 (2007).
[14] P. Ágoston, K. Albe, R. M. Nieminen, and M. J. Puska, Phys. Rev. Lett. **103**, 245501 (2009).
[15] P. Ágoston, P. Erhart, A. Klein, and K. Albe, J. Phys. Condens. Matter **21**, 455801 (2009).
[16] J. Buckeridge, C. R. A. Catlow, M. R. Farrow, A. J. Logsdail, D. O. Scanlon, T. W. Keal, P. Sherwood, S. M. Woodley, A. A. Sokol, and A. Walsh, Phys. Rev. Materials **2**, 054604 (2018).
[17] Q. Hou, J. Buckeridge, T. Lazauskas, D. Mora-Fonz, A. A. Sokol, S. M. Woodley, and C. R. A. Catlow, J. Mater. Chem. C **6**, 12386 (2018).
[18] J. H. W. de Wit, G. Van Unen, and M. Lahey, J. Phys. Chem. Solids **38**, 819 (1977).
[19] J. I. Jeong, J. H. Moon, J. H. Hong, J. S. Kang, and Y. P. Lee, Appl. Phys. Lett. **64**, 1215 (1994).
[20] J. R. Bellingham, A. P. Mackenzie, and W. A. Phillips, Appl. Phys. Lett. **58**, 2506 (1991).
[21] L.-j. Meng and M. P. dos Santos, Appl. Surf. Sci. **120**, 243 (1997).
[22] T. Tomita, K. Yamashita, Y. Hayafuji, and H. Adachi, Appl. Phys. Lett. **87**, 051911 (2005).
[23] N. Preissler, O. Bierwagen, A. T. Ramu, and J. S. Speck, Phys. Rev. B **88**, 085305 (2013).
[24] M. Feneberg, J. Nixdorf, C. Lidig, R. Goldhahn, Z. Galazka, O. Bierwagen, and J. S. Speck, Phys. Rev. B **93**, 045203 (2016).
[25] A. Janotti and C. G. Van de Walle, Phys. Rev. B **76**, 165202 (2007).
[26] A. K. Singh, A. Janotti, M. Scheffler, and C. G. Van de Walle, Phys. Rev. Lett. **101**, 055502 (2008).
[27] F. Oba, A. Togo, I. Tanaka, J. Paier, and G. Kresse, Phys. Rev. B **77**, 245202 (2008).
[28] S. Limpijumnong, P. Reunchan, A. Janotti, and C. G. Van de Walle, Phys. Rev. B **80**, 193202 (2009).
[29] I. Tanaka, K. Tatsumi, M. Nakano, H. Adachi, and F. Oba, J. Am. Ceram. Soc. **85**, 68 (2002).
[30] A. Walsh, J. L. F. Da Silva, S.-H. Wei, C. Körber, A. Klein, L. F. J. Piper, A. DeMasi, K. E. Smith, G. Panaccione, P. Torelli, D. J. Payne, A. Bourlange, and R. G. Egdell, Phys. Rev. Lett. **100**, 167402 (2008).
[31] F. P. Sabino, R. Besse, L. N. Oliveira, S.-H. Wei, and J. L. F. Da Silva, Phys. Rev. B **92**, 205308 (2015).
[32] A. Bourlange, D. Payne, R. Egdell, J. Foord, P. Edwards, M. Jones, A. Schertel, P. Dobson, and J. Hutchison, Appl. Phys. Lett. **92**, 092117 (2008).
[33] K. Irmscher, M. Naumann, M. Pietsch, Z. Galazka, R. Uecker, T. Schulz, R. Schewski, M. Albrecht, and R. Fornari, Phys. Status Solidi A **211**, 54 (2014).
[34] H. Adachi, *DV-Xα Method and Molecular Structure* (Springer, Berlin, 2006).
[35] R. Weiher and R. Ley, J. Appl. Phys. **37**, 299 (1966).
[36] A. Janotti, D. Segev, and C. G. Van de Walle, Phys. Rev. B **74**, 045202 (2006).
[37] P. Reunchan, X. Zhou, S. Limpijumnong, A. Janotti, and C. G. Van de Walle, Curr. Appl. Phys. **11**, S296 (2011).
[38] J. Liu, T. Liu, F. Liu, and H. Li, RSC Adv. **4**, 36983 (2014).
[39] A. Walsh and D. O. Scanlon, Phys. Rev. B **88**, 161201(R) (2013).
[40] W.-J. Yin, J. Ma, S.-H. Wei, M. M. Al-Jassim, and Y. Yan, Phys. Rev. B **86**, 045211 (2012).
[41] Z. G. Yu, J. Sun, M. B. Sullivan, Y.-W. Zhang, H. Gong, and D. J. Singh, Chem. Phys. Lett. **621**, 141 (2015).
[42] J. Heyd, G. E. Scuseria, and M. Ernzerhof, J. Chem. Phys. **118**, 8207 (2003).
[43] J. Heyd, G. E. Scuseria, and M. Ernzerhof, J. Chem. Phys. **124**, 219906 (2006).
[44] P. Àgoston, C. Körber, A. Klein, M. J. Puska, R. M. Nieminen, and K. Albe, J. Appl. Phys. **108**, 053511 (2010).
[45] C. Freysoldt, B. Grabowski, T. Hickel, J. Neugebauer, G. Kresse, A. Janotti, and C. G. Van de Walle, Rev. Mod. Phys. **86**, 253 (2014).
[46] W. Kohn and L. J. Sham, Phys. Rev. **140**, A1133 (1965).
[47] P. E. Blöchl, Phys. Rev. B **50**, 17953 (1994).
[48] G. Kresse and J. Furthmüller, Phys. Rev. B **54**, 11169 (1996).
[49] G. Kresse and D. Joubert, Phys. Rev. B **59**, 1758 (1999).
[50] M. Marezio, Acta Crystallogr. **20**, 723 (1966).
[51] C. Freysoldt, J. Neugebauer, and C. G. Van de Walle, Phys. Rev. Lett. **102**, 016402 (2009).
[52] V. Scherer, C. Janowitz, A. Krapf, H. Dwelk, D. Braun, and R. Manzke, Appl. Phys. Lett. **100**, 212108 (2012).
[53] P. D. C. King, T. D. Veal, F. Fuchs, C. Y. Wang, D. J. Payne, A. Bourlange, H. Zhang, G. R. Bell, V. Cimalla, O. Ambacher *et al.*, Phys. Rev. B **79**, 205211 (2009).
[54] J. A. Dean, *Lange's Handbook of Chemistry* (McGraw–Hill, New York, 1999).

[55] O. Bierwagen and J. S. Speck, Phys. Status Solidi A **211**, 48 (2014).

[56] N. Beji, M. Reghima, M. Souli, and N. Kamoun Turki, J. Alloy Compd. **675**, 231 (2016).

[57] J. B. Varley, A. Janotti, C. Franchini, and C. G. Van de Walle, Phys. Rev. B **85**, 081109(R) (2012).

[58] J. B. Varley, H. Peelaers, A. Janotti, and C. G. Van de Walle, J. Phys. Condens. Matter **23**, 334212 (2011).

[59] E. Korhonen, F. Tuomisto, O. Bierwagen, J. S. Speck, and Z. Galazka, Phys. Rev. B **90**, 245307 (2014).

[60] S. Limpijumnong, X. Li, S.-H. Wei, and S. Zhang, Appl. Phys. Lett. **86**, 211910 (2005).

[61] P. Ágoston and K. Albe, Phys. Rev. B **81**, 195205 (2010).